Periodic Mesoporous Organosilicas with Domain Functionality: Synthesis and Advanced Characterization

James T. A. Jones, Colin D. Wood, Calum Dickinson, and Yaroslav Z. Khimyak*

Department of Chemistry, University of Liverpool, Liverpool L69 7ZD, United Kingdom

Received December 18, 2007. Revised Manuscript Received February 19, 2008

Bifunctional periodic mesoporous organosilicas (PMOs) with $-CH_2-CH_2-$/$-CH=CH-$ bridges have been synthesized using a salt assisted nonionic templating method. The ability to direct locations of the individual organic groups using a novel silica precursor prehydrolysis step is demonstrated. Depending on the prehydrolysis conditions the products showed either structural heterogeneities consisting of domains of the same functionality or a structurally homogeneous system, confirmed by $^1H-^{29}Si$ heteronuclear correlation (HETCOR) experiments. The resulting PMOs show large pore volumes (up to 1.34 $cm^3\ g^{-1}$) and high surface areas (up to 1310 $m^2\ g^{-1}$). The ability to form domain structures within the same mesostructure may have potential applications in molecular recognition and separation.

Introduction

The first syntheses of ordered periodic mesoporous organosilicas (PMOs) with organic groups embedded into the pore walls by the research groups of Stein, Ozin, and Inagaki[1–3] set a new direction in the research of mesoporous molecular sieves. PMO materials are synthesized using bridged organosilica precursors ($(EtO)_3Si-R-Si(OEt)_3$) in conditions analogous to those for the preparation of mesoporous silicas. PMOs offer significant advantages over their mesoporous silica counterparts, that is, MCM-[4] and SBA-type[5,6] materials such as tuneable hydrophobicity and hydrophilicity of the porous network. In comparison with microporous zeolites, PMOs feature increased pore dimensions and the ability to control the molecular recognition properties of the porous network by altering organic functionalities.

Thus far, reported PMOs were synthesized using cationic templates (trialkylammonium[7–9] or pyridinium[10] surfactants) and nonionic surfactants such as oligomeric alkyl poly(ethylene oxide) (PEO), for example, Brij,[11–13] and poly(alkylene oxide) block copolymers, for example, Pluronic.[5,6,14,15] Materials formed using cationic surfactants tend to be synthesized in basic medium via an S^+I^- pathway where the surfactant (S) is positively charged and the silicate species are negatively charged (I) with the governing coassembly interactions being electrostatic.[16] The use of cetylpyridinium chloride templates in acidic medium has been demonstrated. Yet a halide salt is required, and the mesostructured materials are formed via a $S^+X^-I^+$ pathway, where X is a halide such as fluoride, chloride, or bromide and the silicate species are positively charged.[17,18] Solids formed using cationic templates show either two-dimensional (2D) hexagonal or three-dimensional (3D) cubic mesostructures analogous to those of MCM-41 and MCM-48[19] silicas with pore diameters and surface areas in the region of 20−30 Å and 500−1000 $m^2\ g^{-1}$, respectively. Syntheses of PMOs using nonionic surfactants are usually carried out in acidic medium. The addition of inorganic salts results in a coassembly pathway of $S^0(XI)^0$ where the anion of the salt forms an ion pair with the positively charged silicate species although hydrogen bonding remains the main driving force for coassembly. However, if the synthesis is carried out in strongly acidic media (pH < 2, the isoelectric point of the Si-OH bearing inorganic species), a $S^0H^+X^-I^+$ coassembly pathway can also occur as the hydrophilic groups of the surfactant carry

* Corresponding author. E-mail: khimyak@liverpool.ac.uk.

(1) Melde, B. J.; Holland, B. T.; Blanford, C. F.; Stein, A. *Chem. Mater.* **1999**, *11*, 3302–3308.
(2) Asefa, T.; MacLachan, M. J.; Coombs, N.; Ozin, G. A. *Nature* **1999**, *402*, 867–871.
(3) Inagaki, S.; Guan, S.; Fukushima, Y.; Ohsuna, T.; Terasaki, O. *J. Am. Chem. Soc.* **1999**, *121*, 9611–9614.
(4) Beck, J. S.; Vartuli, J. C.; Roth, W. J.; Leonowicz, M. E.; Kresge, C. T.; Schmitt, K. D.; Chu, C. T. W.; Olson, D. H.; Sheppard, E. W.; McCullen, S. B.; Higgins, J. B.; Schlenker, J. L. *J. Am. Chem. Soc.* **1992**, *114*, 10834–10843.
(5) Zhao, D. Y.; Feng, J. L.; Huo, Q. S.; Melosh, N.; Fredrickson, G. H.; Chmelka, B. F.; Stucky, G. D. *Science* **1998**, *279*, 548–552.
(6) Zhao, D. Y.; Huo, Q. S.; Feng, J. L.; Chmelka, B. F.; Stucky, G. D. *J. Am. Chem. Soc.* **1998**, *120*, 6024–6036.
(7) Guan, S.; Inagaki, S.; Ohsuna, T.; Terasaki, O. *J. Am. Chem. Soc.* **2000**, *122*, 5660–5661.
(8) Sayari, A.; Hamoudi, S.; Yang, Y.; Moudrakovski, I. L.; Ripmeester, J. R. *Chem. Mater.* **2000**, *12*, 3857–3863.
(9) Inagaki, S.; Guan, S.; Ohsuna, T.; Terasaki, O. *Nature* **2002**, *416*, 304–307.
(10) Kuroki, M.; Asefa, T.; Whitnal, W.; Kruk, M.; Yoshina-Ishii, C.; Jaroniec, M.; Ozin, G. A. *J. Am. Chem. Soc.* **2002**, *124*, 13886–13895.
(11) Hamoudi, S.; Kaliaguine, S. *Chem. Commun.* **2002**, 2118–2119.
(12) Burleigh, M. C.; Markowitz, M. A.; Spector, M. S.; Gaber, B. P. *J. Phys. Chem. B* **2002**, *106*, 9712–9716.
(13) Wang, W. H.; Xie, S. H.; Zhou, W. Z.; Sayari, A. *Chem. Mater.* **2004**, *16*, 1756–1762.
(14) Guo, W. P.; Kim, I.; Ha, C. S. *Chem. Commun.* **2003**, 2692–2693.
(15) Zhao, L.; Zhu, G. S.; Zhang, D. L.; Di, Y.; Chen, Y.; Terasaki, O.; Qiu, S. L. *J. Phys. Chem. B* **2005**, *109*, 764–768.
(16) Hoffmann, F.; Cornelius, M.; Morell, J.; Froba, M. *Angew. Chem., Int. Ed.* **2006**, *45*, 3216–3251.
(17) Yoshina-Ishii, C.; Asefa, T.; Coombs, N.; MacLachlan, M. J.; Ozin, G. A. *Chem. Commun.* **1999**, 2539–2540.
(18) Temtsin, G.; Asefa, T.; Bittner, S.; Ozin, G. A. *J. Mater. Chem.* **2001**, *11*, 3202–3206.
(19) Vartuli, J. C.; Schmitt, K. D.; Kresge, C. T.; Roth, W. J.; Leonowicz, M. E.; McCullen, S. B.; Hellring, S. D.; Beck, J. S.; Schlenker, J. L.; Olson, D. H.; Sheppard, E. W. *Chem. Mater.* **1994**, *6*, 2317–2326.

10.1021/cm7036124 CCC: $40.75
Published on Web 04/29/2008

a δ^+ charge, thus increasing H-bonding interactions and forming ion pairs with the inorganic salt.[20–22] Solids synthesized using the triblock copolymers P123 or F127 are generally similar in morphology to SBA-15 and SBA-16[5,6] materials respectively possessing pore diameters of 50−100 Å and surface areas in excess of 800 $m^2\ g^{-1}$. The advantages of using triblock copolymers over cationic templates are the increase in wall thickness and, thus, improved hydrothermal stability, and increased pore diameters both in pure silica and in organosilica materials.[5]

Current research in the area of the synthesis of bifunctional PMOs has focused on the incorporation of heteroatoms via isomorphous substitution to expand the range of their various catalytic applications. Aluminum incorporated PMOs have displayed Brønsted acidity[23–25] whereas titanium,[26,27] vanadium,[28] and chromium[29] containing PMOs have shown promise in epoxidation reactions. Other forms of bifunctionality have come in combining bridging ($(EtO)_3Si-R-Si(OEt)_3$) and terminal ($R-Si(OEt)_3$) organosilane precursors. The use of 1,2-bis(triethoxysilyl)ethylene (BTSEY) and triethoxyvinylsilane (TEV) via cationic templating in a basic medium resulted in materials with a 2D hexagonal structure containing vinyl groups embedded in the pore walls and terminal vinyl groups in the pore channels. The presence of vinyl groups in the pore channels clearly reduces the surface area of the products (S_{BET} values of ca. 600 $m^2\ g^{-1}$ are reported).[30] The incorporation of two organic groups into the pore walls has been reported where 1,4-bis(triethoxysilyl)benzene (BTEB) and 2,5-bis(triethoxysilyl)thiophene (BTET) were used to form a 2D hexagonal structure using nonionic templates P123 or Brij76.[31]

The prehydrolysis of the silica source has been used in the preparation of transition metal functionalized PMOs with the main purpose being to equalize the hydrolysis rates of the two precursors.[24] Titania precursors such as titanium chloride or titanium *tert*-butoxide hydrolyze and condense at faster rates than their silica counterparts. Thus prehydrolysis of the silica source (usually tetraethylorthosilicate, TEOS) is required to obtain a homogeneous phase pure Ti-incorporated material.[32] Investigations into the relative hydrolysis/condensation rates of first row transition metals (or metalloid) alkoxides have shown that a triethanolamine ligand (2,2′,2″-nitrilotriethanol) equalizes hydrolysis/condensation rates of various precursors due to its complexing ability.[33,34]

Although the successful incorporation of different organic functionalities within the same mesostructure has been reported in the literature, information on the structure of such solids at a molecular level is still scarce. Recently we studied the dynamics of bifunctional $-CH_2CH_2-$/$-CH=CH-$PMO materials prepared via cationic templating, using cross-polarization kinetics which highlighted changes in the dynamics of the systems between the bifunctional and the monofunctional $-CH_2CH_2-$PMO.[35] However, the ability to direct different functionalities and determine the location of the organic groups in the products has proven difficult in terms of both development of new synthesis strategies and advanced characterization.

In this report we have focused on the preparation of a bifunctional $-CH_2-CH_2-$/$-CH=CH-$PMO using salt assisted nonionic templating in an aqueous acidic medium. We aim to demonstrate that the introduction of a silica precursor prehydrolysis step in the synthetic procedure can alter the properties of the products. The use of joint and separate silica source prehydrolysis protocols can result in different distribution patterns of the organic groups within the porous framework. We also aim to probe the structure of such materials on a molecular level using advanced solid-state NMR to determine the distribution of organic functionalities. Such complex materials may offer uses as solid phases in chromatographic separation and further functionalization leading even to controlled drug delivery systems.

Experimental Section

Synthesis. All starting materials were used as received without further purification: silica precursors, 1,2-bis(triethoxysilyl)ethane (BTSE, 99%, Aldrich), BTSEY (80% trans isomer, 95%, Gelest), Pluronic P123 ($M_w \approx 5800$), sodium chloride (NaCl), hydrochloric acid (36 wt %), and ethanol (98%), all from Aldrich. In a typical synthesis of a $-CH_2CH_2-$/$-CH=CH-$PMO P123 (0.349 g) and NaCl (1.05 g) were dissolved in deionized water (3.0 mL) with a set amount of 2 M HCl(aq) (to give a total of 9 mL after the addition of the prehydrolysis mixture) and stirred until homogeneous at 40 °C. The silica precursors BTSE (0.347 mL) and BTSEY (0.341 mL) were prehydrolyzed either jointly or separately in a set amount of ethanol and 2 M HCl(aq), and time (summarized in Table 1) under stirring at room temperature. After the prehydrolysis the silica solutions were added to the acid/surfactant mixture and stirred vigorously for 24 h at 40 °C. The resulting white suspension was then placed in an autoclave at 80 °C for 24 h. The products were recovered by vacuum filtration, washed sequentially with deionized water and ethanol, and dried at 100 °C. The final composition of the synthesis mixtures was 0.5 BTSE:0.5 BTSEY:0.032 P123:9.6 HCl:9.6 NaCl:344 H_2O.

(20) Tanev, P. T.; Pinnavaia, T. J. *Science* **1995**, *267*, 865–867.
(21) Bagshaw, S. A.; Prouzet, E.; Pinnavaia, T. J. *Science* **1995**, *269*, 1242–1244.
(22) Wan, Y.; Shi, Y. F.; Zhao, D. Y. *Chem. Commun.* **2007**, 897–926.
(23) Hughes, B. J.; Guilbaud, J. B.; Allix, M.; Khimyak, Y. Z. *J. Mater. Chem.* **2005**, *15*, 4728–4733.
(24) Xia, Y. D.; Wang, W. X.; Mokaya, R. *J. Am. Chem. Soc.* **2005**, *127*, 790–798.
(25) Guo, W. P.; Zhao, X. S. *Microporous Mesoporous Mater.* **2005**, *85*, 32–38.
(26) Morishita, M.; Shiraishi, Y.; Hirai, T. *J. Phys. Chem. B* **2006**, *110*, 17898–17905.
(27) Melero, J. A.; Iglesias, J.; Arsuaga, J. M.; Sainz-Pardo, J.; de Frutos, P.; Blazquez, S. *J. Mater. Chem.* **2007**, *17*, 377–385.
(28) Shylesh, S.; Singh, A. P. *Microporous Mesoporous Mater.* **2006**, *94*, 127–138.
(29) Shylesh, S.; Srilakshmi, C.; Singh, A. P.; Anderson, B. G. *Microporous Mesoporous Mater.* **2007**, *99*, 334–344.
(30) Asefa, T.; Kruk, M.; MacLachlan, M. J.; Coombs, N.; Grondey, H.; Jaroniec, M.; Ozin, G. A. *J. Am. Chem. Soc.* **2001**, *123*, 8520–8530.
(31) Morell, J.; Gungerich, M.; Wolter, G.; Jiao, J.; Hunger, M.; Klar, P. J.; Froba, M. *J. Mater. Chem.* **2006**, *16*, 2809–2818.
(32) Chen, Y. Y.; Huang, Y. L.; Xiu, J. H.; Han, X. W.; Bao, X. H. *Appl. Catal., A* **2004**, *273*, 185–191.
(33) Cabrera, S.; El Haskouri, J.; Guillem, C.; Latorre, J.; Beltran-Porter, A.; Beltran-Porter, D.; Marcos, M. D.; Amoros, P. *Solid State Sci.* **2000**, *2*, 405–420.
(34) El Haskouri, J.; de Zarate, D. O.; Guillem, C.; Beltran-Porter, A.; Caldes, M.; Marcos, M. D.; Beltran-Porter, D.; Latorre, J.; Amoros, P. *Chem. Mater.* **2002**, *14*, 4502–4504.
(35) Treuherz, B. A.; Khimyak, Y. Z. *Microporous Mesoporous Mater.* **2007**, *106*, 236–245.

Table 1. Summary of the Pre-Hydrolysis Compositions for Joint and Separate Pre-Hydrolysis Synthesis Mixtures

sample	Si/EtOH	Si/HCl	time (min)
J/S-PMO-0.18-2.6-30	0.18	2.61	30
J/S-PMO-0.18-2.6-60	0.18	2.61	60
J/S-PMO-0.18-14-30	0.18	14.1	30
J/S-PMO-0.18-14-60	0.18	14.1	60
J/S-PMO-0.24-2.6-30	0.24	2.61	30
J/S-PMO-0.24-2.6-60	0.24	2.61	60
J/S-PMO-0.24-14-30	0.24	14.1	30
J/S-PMO-0.24-14-60	0.24	14.1	60
J/S-PMO-0.36-2.6-30	0.36	2.61	30
J/S-PMO-0.36-2.6-60	0.36	2.61	60
J/S-PMO-0.36-14-30	0.36	14.1	30
J/S-PMO-0.36-14-60	0.36	14.1	60
J/S-PMO-0.72-2.6-30	0.72	2.61	30
J/S-PMO-0.72-2.6-60	0.72	2.61	60
J/S-PMO-0.72-14-30	0.72	14.1	30
J/S-PMO-0.72-14-60	0.72	14.1	60

The organic template was removed by acid extraction. Typically 0.30 g of as-synthesized material was stirred in 100 mL of 1 M HCl/EtOH at 50 °C for 24 h. The suspension was cooled, vacuum filtered, with the resulting white solid, was washed using deionized water and EtOH, and then dried at 100 °C for 24 h.

In total 33 products were synthesized: 16 prepared using joint silica precursor prehydrolysis, 16 prepared using separate silica precursor prehydrolysis, and one material prepared using no prehydrolysis to act as a reference. Other synthetic variables were ethanol content, silica/water rati,o and time for the prehydrolysis step. The products are labeled according to their prehydrolysis conditions, *A*-PMO-*X*-*Y*-*Z* where A = J (joint prehydrolysis) or S (separate prehydrolysis), X = 0.18, 0.24, 0.36, or 0.72 indicating Si/EtOH ratio, Y = 14 or 2.6, the Si/HCl ratio, and Z = 30 or 60 min (prehydrolysis time). For example S-PMO-0.18-2.6-30 means separate prehydrolysis was used with Si/EtOH = 0.18, Si/HCl = 2.6, and prehydrolysis for 30 min prior to addition to the acid/surfactant solution.

Characterization. *Powder X-ray Diffraction.* Powder X-ray diffraction (PXRD) patterns were measured using a Panalytical X-pert pro diffractometer with Co Kα_1 radiation with a wavelength λ = 1.789 Å. Patterns were measured in the 0.7−5.0° 2θ range using a flat bracket sample holder.

Nitrogen Adsorption. Nitrogen adsorption−desorption isotherms were measured on a Micromeritics ASAP2420 system at −196 °C. The samples were dried and evacuated for 5 h at 120 °C before analysis. The specific surface area was calculated using the BET method using a linear plot over a range of $p/p_0 = 0.06-0.20$. The pore size distribution was calculated using the adsorption branch of the isotherm using the Barrett−Joyner−Halenda (BJH) method. Pore volume was calculated from the amount of adsorbed nitrogen at $p/p_0 = 0.99$. Micropore volume and surface areas were obtained from the *t*-plot method using a Harkins-Jura reference isotherm ($t = (13.99/(0.034 - \log p/p_s))^{1/2}$).

Electron Microscopy. Samples for transmission electron microscopy (TEM) were prepared by grinding the powder in alcohol, and a drop of the suspension was deposited onto a holey carbon film, supported by a copper grid. High-resolution electron microscopy (HREM) was performed using a JEOL 2011 microscope with a laboratory filament and a point resolution of 1.8 Å (acceleration voltage = 200 kV).

Solid-State NMR. Solid-state NMR experiments were conducted at 9.4 T using a Bruker DSX-400 spectrometer equipped with either a 4 mm ^{1}H/X/Y or 2.5 mm ^{1}H/^{19}F/X probes.

^{1}H magic angle spinning (MAS) NMR spectra were acquired at 400.16 MHz with a ^{1}H π/2 pulse length of 2.8 μs at a MAS rate of 30.0 kHz and a recycle delay of 15 s. The position of the ^{1}H resonances is quoted in ppm from external tetramethylsilane (TMS).

The ^{1}H−^{13}C cross-polarization (CP) MAS NMR spectra were acquired at 400.16 MHz for ^{1}H and 100.56 MHz for ^{13}C at MAS rate of 8.0 kHz. A ^{1}H π/2 pulse length was 3.0 μs, and the recycle delay was 8.0 s. Two phase pulse modulation (TPPM) decoupling[36] was used during acquisition. The CP contact time was 1.0 ms with the Hartman−Hahn matching condition set using hexamethylbenzene (HMB). The ^{13}C chemical shifts are quoted in ppm with respect to TMS. ^{1}H−^{13}C variable contact time (VCT) CP/MAS NMR spectra were acquired using contact times in the range of 0.01−16.0 ms. The data points were fitted using a two populations model derived from the classical I−S model.[37]

^{1}H−^{29}Si CP MAS NMR spectra were acquired at 400.16 MHz for ^{1}H and 78.5 MHz for ^{29}Si at a MAS rate of 4.0 kHz. A ^{1}H π/2 pulse length of 3.1 μs and a recycle delay of 10 s with TPPM decoupling were used during acquisition. The CP contact time was 2.0 ms with the Hartmann−Hahn matching condition set using kaolinite. The ^{29}Si chemical shifts are quoted in ppm with respect to TMS. The ^{1}H−^{29}Si VCT/CP MAS NMR measurements used contact times ranging from 0.05 to 12.0 ms. The data were fitted according to the I−S model.[37]

^{29}Si single pulse (SP) MAS NMR spectra were acquired at 78.5 MHz at a MAS rate of 4.0 kHz. A ^{29}Si π/3 pulse length of 2.3 μs and a recycle delay of 240 s without proton decoupling were used for acquisition. The ^{29}Si chemical shifts are quoted in ppm with respect to TMS.

2D ^{1}H−^{29}Si heteronuclear correlation (HETCOR)[38] MAS NMR spectra were acquired at 400.16 MHz for ^{1}H and 78.5 MHz for ^{29}Si with a MAS rate of 10 kHz. The 2D HETCOR experiments used frequency-switched Lee−Goldburg (FSLG)[39,40] homonuclear decoupling with a ^{1}H *rf* field of approximately 80.6 kHz in t_1 and ramp amplitude ^{1}H−^{29}Si CP with a contact time of 2.0 ms. TPPM decoupling was used during acquisition at a decoupling strength of approximately 80.6 kHz. The sample volume was restricted to the middle of the rotor to improve the *rf* homogeneity. States-TPPI was employed for phase sensitive detection.[41–44] The recycle delay was set at 2.0 s. 256 increments were recorded in t_1 to cover the full ^{1}H spectral width, with 600 scans acquired in t_2 per increment.

Results and Discussion

Synthetic Observations. The synthesis of PMOs relies on the self-assembly of surfactant template and organosilicate secondary building units (SBU) formed via the hydrolysis and condensation of initial organosilane precursors.[16,22] The joint hydrolysis mixtures consisted of both −CH_2−CH_2− and −CH=CH− bridged precursors in appropriate amounts of 2 M HCl and ethanol in the

(36) Bennett, A. E.; Rienstra, C. M.; Auger, M.; Lakshmi, K. V.; Griffin, R. G. *J. Chem. Phys.* **1995**, *103*, 6951–6958.
(37) Kolodziejski, W.; Klinowski, J. *Chem. Rev.* **2002**, *102*, 613–628.
(38) vanRossum, B. J.; Forster, H.; deGroot, H. J. M. *J. Magn. Reson., Ser. A* **1997**, *124*, 516–519.
(39) Bielecki, A.; Kolbert, A. C.; Levitt, M. H. *Chem. Phys. Lett.* **1989**, *155*, 341–346.
(40) Laws, D. D.; Bitter, H. M. L.; Jerschow, A. *Angew. Chem., Int. Ed.* **2002**, *41*, 3096–3129.
(41) States, D. J.; Haberkorn, R. A.; Ruben, D. J. *J. Magn. Reson., Ser. A* **1982**, *48*, 286–292.
(42) Keeler, J.; Neuhaus, D. *J. Magn. Reson., Ser. A* **1985**, *63*, 454–472.
(43) Levitt, M. H. *Spin Dynamics: Basics of Nuclear Magnetic Resonance*; John Wiley & Sons Ltd.: New York, 2001.
(44) Keeler, J. *Understanding NMR Spectroscopy*; John Wiley & Sons Ltd.: New York, 2005.

Scheme 1. Formation of Homo- and Hetero-Organo-Functionalised SBUs and the Resulting Bifunctional PMOs Prepared Using the Joint and Separate Pre-Hydrolysis Protocols

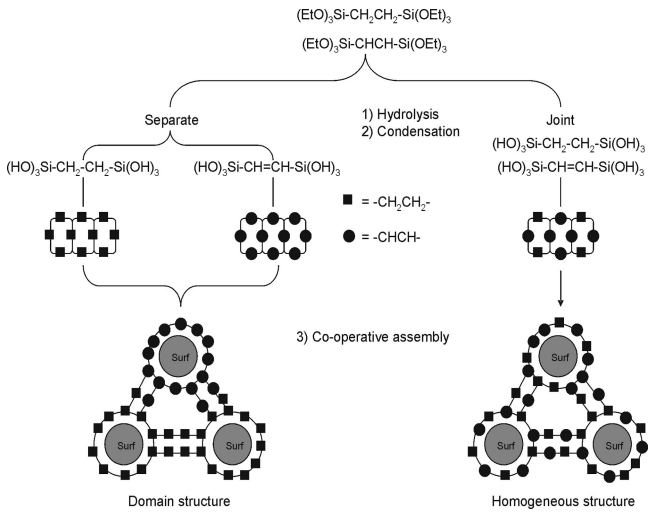

same container. Synthesis mixtures with identical Si/HCl and Si/C_2H_5OH ratios were used in separate prehydrolysis protocols when the precursors with different organic bridges were combined only at the stage of addition to the template solution. The introduction of joint and separate prehydrolysis of the silica precursors could facilitate the formation of homo- and hetero-organo-functionalized SBUs prior to self-assembly with the template. The formation of two types of organo-functionalized SBUs might affect the overall distribution of organic groups in the products (Scheme 1). This will be probed using advanced characterization methodologies sensitive to the local organization in solids with limited long-range ordering.

The prehydrolysis protocols were used to find an optimum balance between size of the SBUs and their ability to undergo the self-assembly with the template required to form ordered porous materials. Clearly, once traces of the bulk amorphous organosilane product are formed (i.e., the case of very large SBUs), their assembly with the template is restricted. Although direct measurements of the sizes of SBUs are beyond the scope of this report, indirect conclusions can be made from observations of the hydrolysis mixtures. The latter are consistent with previous studies on the hydrolysis/condensation rates and resulting particle sizes of TEOS in $H_2O/EtOH/HCl$ solutions.[45]

The hydrolysis of metal (or metalloid) alkoxides can be promoted using either acidic or basic catalysts. The mechanism of hydrolysis is based on the nucleophilic attack at the electropositive metal center. Once the water ligand is bound to the metal, proton transfer to the leaving alkoxy group occurs.[46,47] The condensation of metal alkoxides proceeds either through water or alcohol elimination reactions leading to the formation of metal−oxygen−metal bonds (equations below).

$$\text{Si—OH} + \text{HO—Si} \rightarrow \text{Si—O—Si} + H_2O$$

$$\text{Si—OR} + \text{HO—Si} \rightarrow \text{Si—O—Si} + \text{ROH}$$

For alkoxysilanes, the rate of hydrolysis is dependent on several factors, such as the nature of the organic bridging group, temperature, time, and Si/acid ratio. The relative hydrolysis/condensation rates of the two organosilane precursors were found to be different and, generally, the —CH=CH— bridged precursor hydrolyzed/condensed faster than the one with $-CH_2-CH_2-$ groups. Viscous gels and eventually white rigid solids encapsulating the solvent were obtained in the separately prehydrolyzed mixtures with high Si/EtOH ratios containing only BTSEY. As the C=C double bond is more electron rich compared to C—C single bond, the silicon atoms in BTSEY are more susceptible to nucleophilic attack from water causing hydrolysis rates to increase according to the principle of "electronegativity equilization".[48] The increase in positive charge on the silicon atoms of $(H_5C_2O)_3—Si—CH=CH—Si(OC_2H_5)_3$ is also evident from the ^{29}Si NMR data (discussed later) as the ^{29}Si resonances attributed to $-HC=CH-SiO_3$ environments appear downfield compared to chemical shifts of silicon sites in the $-CH_2-CH_2-SiO_3$ units.

A key factor controlling the rates of hydrolysis/condensation was the ethanol content in the prehydrolysis mixtures. The jointly and separately prehydrolyzed synthesis mixtures with a Si/EtOH = 0.18 remained clear solutions. As the ethanol content was reduced to Si/EtOH = 0.24 an increase in hydrolysis/condensation rates was observed. The synthesis mixture with —CH=CH— bridged precursor resulted in a cloudy viscous solution after 60 min (Si/HCl = 14.1). The analogous synthesis mixture with $-CH_2-CH_2-$ bridged organosilane remained clear and colorless, though its viscosity increased after 60 min. A further reduced content of ethanol (Si/EtOH = 0.72) resulted in both the jointly and the separately hydrolyzed mixtures forming white solids after 5 min irrespectively of the HCl content. These observations can be explained by the molecular separation effect reported for $Si(OC_2H_5)_4/HCl/C_2H_5OH$ systems.[45,49] Diluting the hydrolysis mixtures with ethanol increases the separation of the silica precursors and water within the solution thus slowing down the rates of hydrolysis/condensation.

The effect of the Si/HCl ratio on the rates of hydrolysis/condensation is evident from the separately prehydrolyzed solutions with Si/EtOH = 0.24. Both BTSE and BTSEY solutions remain clear when Si/HCl = 14.1. However, when Si/HCl = 2.6 the BTSEY mixture became a cloudy viscous solution. With HCl acting as a homogeneous catalyst it is clear that increasing its content in the reaction medium increases the rates of hydrolysis/condensation.

PXRD. The $-CH_2-CH_2-$/—CH=CH—PMO prepared without prehydrolysis of the silica source displayed PXRD patterns typical of a 2D hexagonal SBA-15 type phase with a sharp reflection (d_{100} = 92.5 Å). The value of d_{100} increased to 97.0 Å after removal of the template. The degree of mesoscopic ordering is reduced in all prehydrolyzed products (Figure 1 and Supporting Information, Figures S1 and S2) compared to the reference PMO indicated by the much

(45) Yoldas, B. E. *J. Non-Cryst. Solids* **1986**, *83*, 375–390.
(46) Livage, J.; Henry, M.; Sanchez, C. *Prog. Solid State Chem.* **1988**, *18*, 259–341.
(47) Barringer, E. A.; Bowen, H. K. *Langmuir* **1985**, *1*, 414–420.
(48) Sanderson, R. T. *Science* **1951**, *114*, 670–672.
(49) Yoldas, B. E. *J. Non-Cryst. Solids* **1986**, *82*, 11–23.

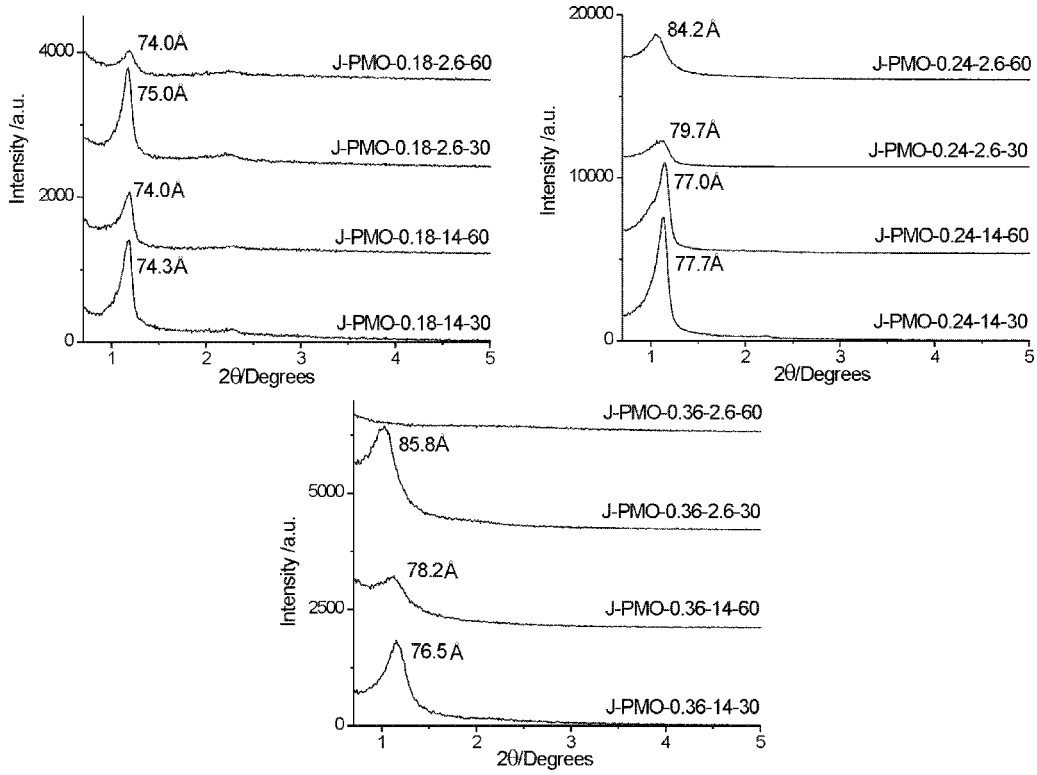

Figure 1. PXRD patterns of the as-synthesised PMOs prepared using the joint prehydrolysis protocols.

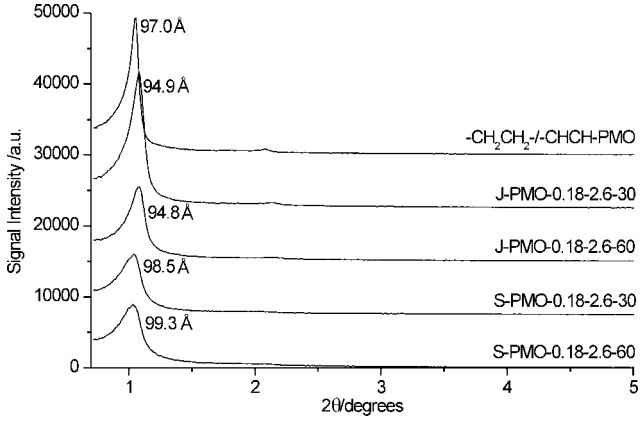

Figure 2. PXRD patterns of the template extracted PMOs.

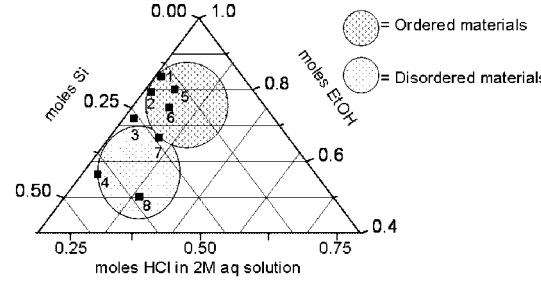

Figure 3. Composition of the prehydrolysis mixtures in terms of silica/ethanol/HCl(aq) ratio. (1) PMO-0.18-14, (2) PMO-0.24-14, (3) PMO-0.36-14, (4) PMO-0.72-14, (5) PMO-0.18-2.6, (6) PMO-0.24-2.6, (7) PMO-0.36-2.6, and (8) PMO-0.72-2.6.

broader low angle reflections. This is consistent with formation of larger SBU (see above) interacting with the template and assembling into surfactant−organosilica hybrids with lower degree of mesoscopic ordering. The J-PMOs show a broad reflection with d_{100} = 74.3−85.8 Å. The peak is shifted to lower angle (d_{100} = 87.3−93.9 Å) for products prepared using separate prehydrolysis. The broader reflections for the S-PMOs suggest a reduced mesoscopic ordering with respect to their jointly prehydrolyzed counterparts.

The PXRD patterns of the template extracted products (Figure 2 and Supporting Information, Figures S3 and S4) display a significant increase of the intensity typical for mesoporous silicas.[50] The narrowing of the reflections upon the template extraction indicates a slight increase in long-range ordering. The d_{100}-spacings for the J-PMOs increased from approximately 85.8 to 95.5 Å upon surfactant extraction, although no change in d_{100}-spacings was observed for the separately prehydrolyzed materials. Such an increase was not accompanied by a change in the degree of condensation of pore walls derived from the $^{1}H-^{29}Si$ CP/MAS NMR spectra (see below).

The degree of mesoscopic ordering is affected by the composition of prehydrolysis solution. The regions of formation of the ordered and disordered materials as a function of Si/EtOH/HCl (2 M aqueous solution) are indicated in Figure 3. A decrease in mesoscopic ordering as the Si/EtOH ratio increases in the prehydrolysis mixtures is observed. Very rapid hydrolysis/condensation rates of the organosilane precursors at Si/EtOH = 0.72 prevent effective self-assembly of the preformed large SBUs with the template and lead to products with no mesoscopic ordering (Supporting Information, Figures S1d and Figure S2d). A general decrease in mesoscopic ordering was observed as the prehydrolysis time increased from 30 to 60 min (Figure 1a–c

(50) Zhu, H.; Jones, D. J.; Zajac, J.; Dutartre, R.; Rhomari, M.; Roziere, J. *Chem. Mater.* **2002**, *14*, 4886–4894.

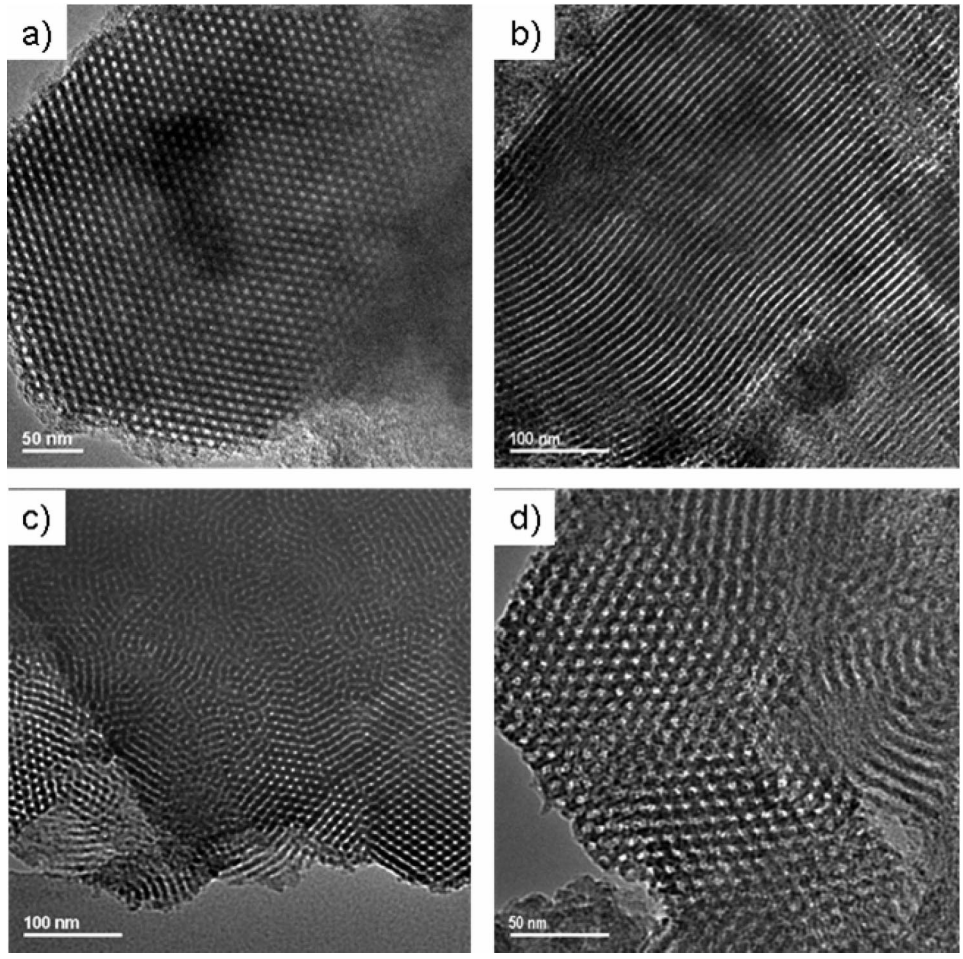

Figure 4. TEM images of the template extracted PMOs: (a) —CH_2CH_2—/—CHCH—PMO view parallel to the pores, (b) —CH_2CH_2—/—CHCH—PMO view perpendicular to the pores, (c) J-PMO-0.18-2.6-30, and (d) S-PMO-0.18-2.6-30.

and Supporting Information, Figure S2a). These observations indicate that a balance between the concentration of SBUs and their size is required to form an ordered PMO.

The effect of the Si/HCl on the ordering of the materials is dependent on the Si/EtOH ratio. At high ethanol concentrations, an increase in HCl content in the hydrolysis mixture has little effect on the ordering of the resulting products (Figure 1a). However, as the ethanol content is decreased an increase in HCl concentration causes a reduction in the overall ordering of the products (Figure 1b). This observation is again closely linked to the molecular separation effect discussed above.

The salt assisted templating using nonionic surfactants in strong acidic media can be classified as a $S^0H^+X^-I^+$ pathway where the Cl^- ions form ion pairs with $\equiv Si(OH_2)^+$ species as well as the protonated PEO group of the surfactant with the driving force for co-operative assembly being H-bonding and ion pairing. This pathway remains valid for the selected range of prehydrolysis conditions, although in the system under study it appears less effective as the concentration of reactive $\equiv Si(OH_2)^+$ species is reduced as a result of the formation of large SBUs, hence leading to the less ordered materials (Supporting Information, Figures S1d and S2d).

Transmission Electron Microscopy (TEM). The hexagonal symmetry of the —CH_2—CH_2—/—CH═CH—PMOs prepared without and with joint or separate prehydrolysis was confirmed by TEM images (Figure 4). The parallel view to the pores of the —CH_2—CH_2—/—CH═CH—PMO (Figure 4a) shows a honeycomb-like structure while the perpendicular view (Figure 4b) shows a well ordered material with well defined pore channels. The TEM image for the jointly prehydrolyzed product J-PMO-0.18-2.6-30 (Figure 4c) indicates a structure similar to that of the reference material (Figure 4a), yet the honeycomb-like arrangement is distorted. The TEM image of the separately prehydrolyzed material S-PMO-0.18-2.6-30 shows two distinct pore domains in the mesoporous framework, suggesting preferential distribution of —CH_2—CH_2— and —CH═CH— functional groups. The presence of such domains results in distorted hexagonal arrangement of pores leading to broadening of PXRD reflections for products obtained using both separate and joint prehydrolysis protocols (Figure 4). All images for the bifunctional PMOs indicate that the materials are phase pure with no separation into two frameworks being observed. The unit cell parameter a of the mesostructure, estimated from the TEM images (ca. 87.6 Å), is in good agreement with the XRD results. The PXRD patterns and TEM images show that well ordered PMO materials are formed using the prehydrolysis methods and possess hexagonal symmetry.

Nitrogen Adsorption—Desorption Isotherms. Nitrogen adsorption—desorption isotherms provide information on the

Table 2. Textural Properties of Surfactant Extracted Bifunctional PMOs[a]

sample	S_{BET}, $m^2\ g^{-1}$	V_{ads}, $cm^3\ g^{-1}$	D_{AV}^{ads}, Å	d_{100}, Å	a,[b] Å	W, Å	mV_{ads},[c] $cm^3\ g^{-1}$	mS,[c] $m^2\ g^{-1}$
CH_2CH_2/CHCH—PMO	1040	1.04	65.3	97.0	112	46.7	0.101	248
J-PMO-0.18-14-30	1310	1.34	57.4	94.0	109	51.1	0.139	336
J-PMO-0.18-14-60	1290	1.27	54.4	89.0	103	48.4	0.125	307
J-PMO-0.18-2.6-30	1290	1.23	61.6	94.9	110	48.0	0.125	308
J-PMO-0.18-2.6-60	1170	1.08	57.7	94.8	109	51.7	0.105	263
J-PMO-0.24-14-30	1130	1.13	58.0	96.8	112	53.8	0.113	276
J-PMO-0.24-14-60	994	0.88	54.9	93.5	108	53.1	0.137	319
S-PMO-0.18-14-30	997	1.14	61.1	96.9	112	50.8	0.097	236
S-PMO-0.18-2.6-30	946	0.97	61.1	98.5	114	52.6	0.092	224
S-PMO-0.18-2.6-60	904	0.93	65.4	99.3	115	49.3	0.077	192
S-PMO-0.24-14-30	978	1.24	61.5	96.3	111	49.7	0.057	154
S-PMO-0.24-14-60	943	1.05	57.8	96.2	111	53.3	0.067	173

[a] Pore volumes determined at $p/p_0 = 0.9$. W is wall thickness determined from $\bar{a} - D_{av}$. [b] Unit cell parameter $\bar{a}$ determined from d_{100} values using $\bar{a} = 2d_{100}/\sqrt{3}$. [c] Micropore volume and surface area determined using the t-plot method.

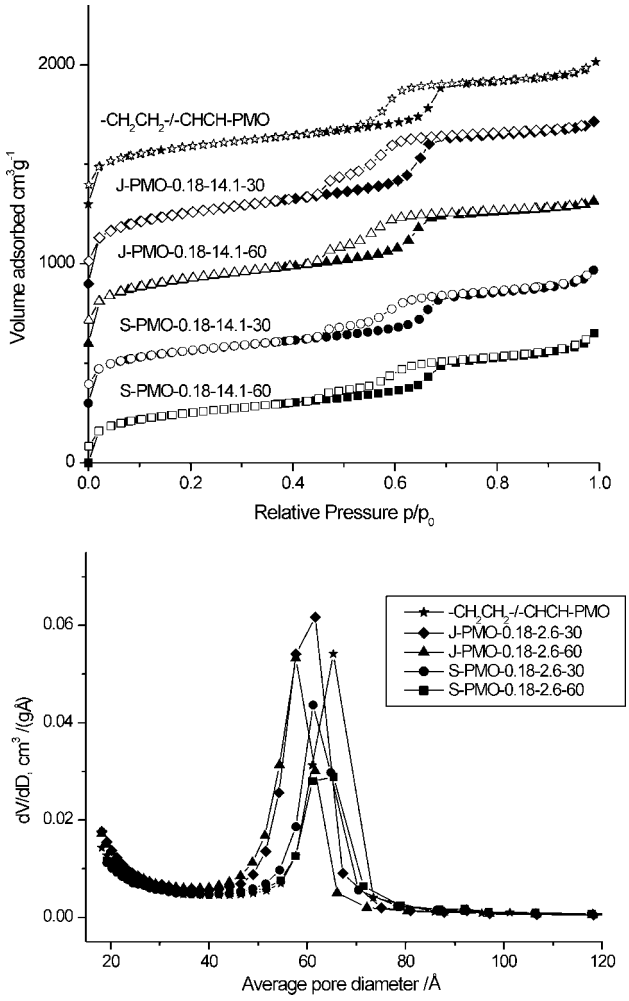

Figure 5. Nitrogen adsorption−desorption isotherms of surfactant extracted PMOs (top). Pore size distribution plots calculated from the adsorption branch of the N_2 isotherms (bottom).

textural properties and mesoscopic quality of PMOs. The bifunctional —CH_2—CH_2—/—CH═CH—PMOs display high surface areas and large pore volumes (Table 2). Consistently with the results of PXRD, the reference —CH_2—CH_2—/—CH═CH—PMO (Figure 5) shows the highest degree of mesoscopic ordering with the sharpest capillary condensation step on the adsorption branch ($p/p_o \approx 0.65$). The adsorption/desorption isotherm can be described as a type IV isotherm with a type H1 hysteresis. Type H1 hystereses indicate that the material possesses cylindrical pores of uniform size and shape.

The majority of products prepared using the prehydrolysis step showed isotherms similar to that for the reference compound. However, in agreement with results of PXRD, the overall degree of ordering is reduced. The BET surface areas, total pore volumes, micropore volumes and micropore areas for the jointly prehydrolyzed materials are higher than for their separately prehydrolyzed analogues. The nitrogen adsorption−desorption isotherms and pore size distribution curves of the jointly prehydrolyzed materials show a narrow pore size distribution with average pore diameters of approximately 57 Å determined from the adsorption branch of the isotherm. The material J-PMO-0.24-14-60 shows a type H2 hysteresis suggesting cylindrical pores of a nonuniform shape such as ink-bottle type pores and size.

The adsorption−desorption isotherms for the separately prehydrolyzed materials confirmed a decrease in mesoscopic ordering upon the decrease in ethanol content during the prehydrolysis. The desorption branch on the isotherms of S-PMO-0.18-2.6-30 and S-PMO-0.18-2.6-60 show a second step at $p/p_0 = 0.45$. Such a step is also present on the isotherms of J-PMO-0.18-2.6-30 and J-PMO-0.18-2.6-60. This may result from two different pore openings present in the materials as previous studies of mesoporous silicas have shown changes in hystereses as a function of pore openings.[51] For example, large pore cubic ($Fm3m$) mesoporous silicas with different pore openings displayed either H1 or H2-type hystereses. Van Der Voort et al. also observed a second desorption step at $p/p_0 = 0.45$ and explained it as a direct result of pore blocking.[52] The interpretation that blocked pores remain filled until the vapor pressure is lowered ($p/p_0 = 0.45$), after which a cavitation of the condensed N_2 occurs, and closed sections spontaneously empty is supported by nonlocal density functional theory (NLDFT) of adsorption and hysteresis in cylindrical pores.[53,54] The separately prehydrolyzed materials (Figure 5) show a narrow pore size distribution with a maximum at approximately 62 Å which

(51) Fan, J.; Yu, C. Z.; Lei, J.; Zhang, Q.; Li, T. C.; Tu, B.; Zhou, W. Z.; Zhao, D. Y. *J. Am. Chem. Soc.* **2005**, *127*, 10794–10795.
(52) Van Der Voort, P.; Ravikovitch, P. I.; De Jong, K. P.; Benjelloun, M.; Van Bavel, E.; Janssen, A. H.; Neimark, A. V.; Weckhuysen, B. M.; Vansant, E. F. *J. Phys. Chem. B* **2002**, *106*, 5873–5877.
(53) Van Der Voort, P.; Ravikovitch, P. I.; De Jong, K. P.; Neimark, A. V.; Janssen, A. H.; Benjelloun, M.; Van Bavel, E.; Cool, P.; Weckhuysen, B. M.; Vansant, E. F. *Chem. Commun.* **2002**, 1010–1011.
(54) Neimark, A. V.; Ravikovitch, P. I.; Vishnyakov, A. *Phys. Rev. E* **2000**, *62*, R1493–R1496.

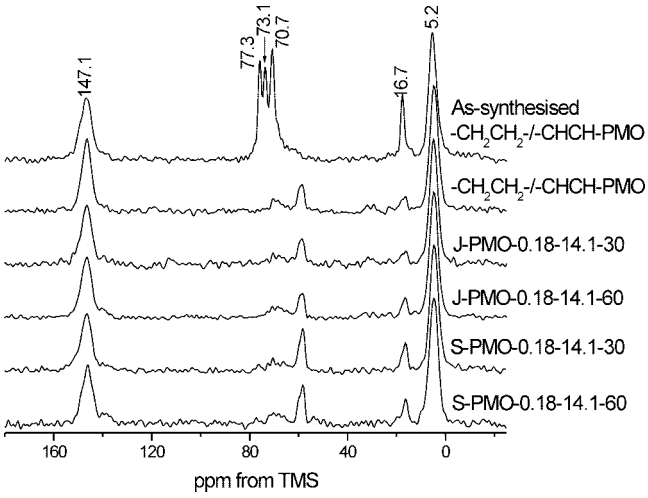

Figure 6. $^{1}H-^{13}C$ CP/MAS NMR spectra of the as-synthesised (top) and template extracted PMOs.

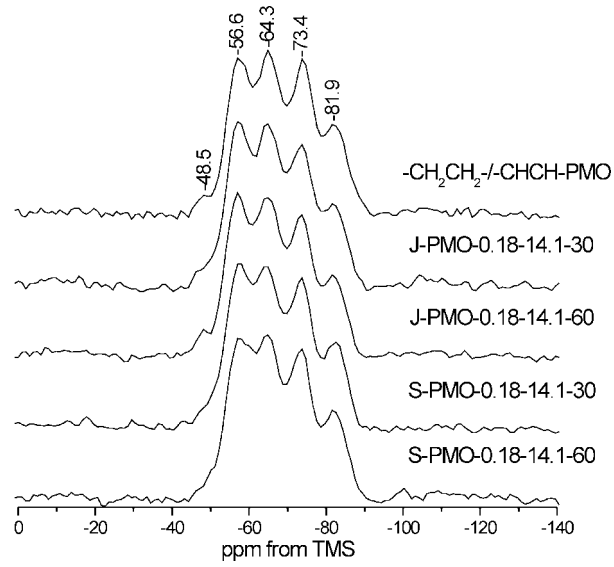

Figure 7. $^{1}H-^{29}Si$ CP/MAS NMR spectra of the template extracted PMOs.

becomes increasingly broader as the ethanol content is reduced and the prehydrolysis time is increased.

The results of N_2 adsorption are in good agreement with conclusions about mesoscopic ordering of the products derived from the PXRD. Although PXRD and nitrogen adsorption are capable of determining the overall mesoscopic ordering and textural properties of bifunctional PMOs, these methods are limited in probing the molecular level structure of such materials. Obtaining such information, to determine the composition, location, and mobility of organic functionalities within the pore walls of PMOs, is particularly challenging because of their amorphous frameworks.

Composition of PMO from Solid-State NMR. $^{1}H-^{13}C$ CP/MAS NMR was used to determine the presence of organic functionalities in the framework and assess the efficiency of template extraction. The NMR spectrum of the as-synthesized $-CH_2-CH_2-/-CH=CH-$PMO (Figure 6, top spectrum) displays two broad resonances attributed to $-CH_2-CH_2-$ (5.2 ppm) and $-CH=CH-$ (147.1 ppm) bridges in the framework. These resonances remain unchanged upon surfactant extraction (Figure 6). Other resonances in the spectra of the as-synthesized PMO are attributed to the pluronic surfactant: the peak at 16.7 ppm corresponds to the $-CH_3$ group of the PPO block; the peak at 70.7 ppm is attributed to PEO blocks; the resonances at 73.1 and 77.3 ppm correspond to CH_2 and CH sites of PPO blocks, respectively.[55] In general, the surfactant peaks are narrower than those of the organic bridges, indicating a higher mobility of the surfactant PEO−PPO−PEO blocks typical of surfactant−organosilica materials.[35] The acid extraction was sufficient to remove the majority of the template. However, the process becomes less efficient as the ethanol content in in the synthesis mixtures decreases. The two resonances at 16.4 and 59.1 ppm in the spectra of the template extracted products result from the residual ethoxy groups located on the pore surface due to the extraction process.

(55) Steinbeck, C. A.; Hedin, N.; Chmelka, B. F. *Langmuir* **2004**, *20*, 10399–10412.

$^{1}H-^{29}Si$ CP/MAS NMR spectra of PMOs indicate the degree of condensation of the hybrid organosilica framework and confirm the types of silicon environments present. The $^{1}H-^{29}Si$ CP/MAS NMR spectra (Figures 7 and Supporting Information, Figures S9 and S10) exhibit a weak resonance at −48.5 ppm corresponding to the poorly condensed T^1 sites ($R-\mathbf{Si}(OSi)(OH)_2$, $R = -CH_2CH_2-$). The four strong resonances are assigned as follows: the lines at −56.6 and −73.4 ppm correspond to the partially condensed T^2 sites ($R-\mathbf{Si}(OSi)_2(OH)$) while the resonances at −64.3 and −81.9 ppm are assigned to fully condensed T^3 sites ($R-\mathbf{Si}(OSi)_3$) ($R = -CH_2CH_2-$ and $-CH=CH-$, respectively). The T^2 sites are typically located at the pore wall interface whereas the T^3 sites constitute the bulk of the hybrid pore walls. There was no evidence of any Si−C bond cleavage upon acid extraction as no Q^n species were observed in the region from −90 to −120 ppm both for the as-synthesized and the extracted solids. The degree of condensation and relative intensity of the silicon sites remained unchanged upon surfactant extraction confirming that no major changes in local structure occurred.

^{29}Si MAS NMR spectra (Supporting Information) provided quantitative information on the composition of the PMO walls. The degree of condensation ($(T^1 + T^2)/T^3$) was determined using deconvolution of the spectra (Supporting Information). In general, the silicon sites connected to the $-CH=CH-$ groups are less condensed than the one with attached $-CH_2-CH_2-$ bridges. This observation confirms the tendency of $-CH=CH-$ bridges to be located at the pore wall interface. The $-CH_2-CH_2-/-CH=CH-$ ratio ≈ 1, determined from the ^{29}Si MAS NMR spectra, is in good agreement with the original synthesis composition.

Fast ^{1}H MAS NMR (25−30 kHz) provides sufficient resolution to assess the proton environments present in the PMOs. Main ^{1}H resonances at 1.2 and 6.9 ppm are attributable to organic bridges $-CH_2CH_2-$ and $-CH=CH-$, respectively (Figure 8). The resonance at 4.2 ppm is due to the H-bonded water and free water molecules trapped within

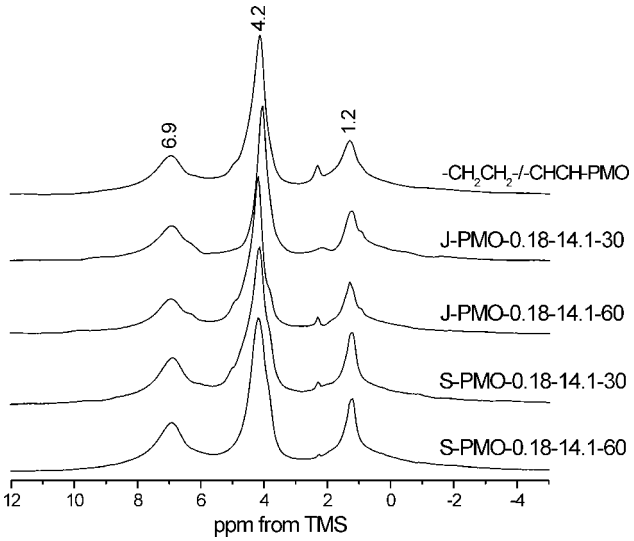

Figure 8. ^{1}H MAS NMR spectra of the template extracted PMOs.

the porous framework. The relatively narrow ^{1}H lines indicate that MAS rates above 25 kHz provide efficient ^{1}H−^{1}H homonuclear decoupling, indicating a high degree of mobility in the products.[56]

The results of solid-state NMR described so far along with PXRD, nitrogen adsorption isotherms, and TEM results suggest that well ordered mesoporous materials have been obtained. However, these results cannot confirm unambiguously that the PMOs formed are phase pure; that is, both organic functionalities are incorporated into the same framework. Determination of phase purity of a bifunctional PMO with amorphous frameworks is only possible via the application of more advanced NMR methods. VCT CP/MAS and HETCOR NMR were used to probe the dynamics of the pore walls and the distribution of the organic functionalities within the framework. The detailed analysis of the structure and dynamics was performed for selected solids obtained using different prehydrolysis protocols: −CH_2CH_2−/−CH=CH−PMO, J-PMO-0.18-2.6-30, J-PMO-0.18-2.6-60, S-PMO-0.18-2.6-30, and S-PMO-0.18-2.6-60. These materials will be referred to as *X*-PMO-*Y* where X = J or S (joint or separate prehydrolysis) and Y = 30 or 60 min (prehydrolysis time) for simplification.

^{1}H−^{13}C VCT CP/MAS NMR. VCT measurements are invaluable for studying structure and dynamics of complex materials and have been widely used to study polymer composites,[57] aluminophosphates,[58,59] and mesoporous silicas[60] including PMO.[35] For the latter, such measurements were used to probe locations of the organic functionalities in the hybrid network.[35]

The kinetics of CP can be described using different models depending on the strength of the ^{1}H−^{1}H homonuclear dipolar coupling. The classical I−S model is ideal for homogeneous solids, where the I−S heteronuclear dipolar interactions are weak and the I−I homonuclear interactions are strong enough to provide an efficient ^{1}H−^{1}H spin diffusion. For a system of an abundant and a dilute spin-$^1/_2$ nucleus, the I−S model leads to the kinetic equation:

$$I(t) = I_0\left(1 + \frac{T_{IS}}{T_{1\rho}^S} - \frac{T_{IS}}{T_{1\rho}^I}\right)^{-1}\left[\exp\left(-\frac{t}{T_{1\rho}^I}\right) - \exp\left(-t\left(\frac{1}{T_{IS}} + \frac{1}{T_{1\rho}^S}\right)\right)\right] \quad (1)$$

where I_0 is the absolute signal intensity; $T_{1\rho}$ is the relaxation time in the rotating frame; and T_{IS} is the CP time constant. For dilute spins, generally one assumes that $T_{IS}/T_{1\rho}^S \rightarrow 0$, and the CP dynamics can be described by the eq 2:

$$I(t) = I_0\left(1 - \frac{T_{IS}}{T_{1\rho}^I}\right)^{-1}\left[\exp\left(-\frac{t}{T_{1\rho}^I}\right) - \exp\left(-\frac{t}{T_{IS}}\right)\right] \quad (2)$$

The T_{IS} time constant is related to internuclear distances and molecular mobility. $T_{1\rho}^H$ relaxation time describes the decay of signal intensity as a function of contact time. The relaxation of the protons in the rotating frame is ensured mostly by ^{1}H−^{1}H homonuclear dipolar interactions. The T_{IS} time is characteristic of particular functional groups under study whereas the $T_{1\rho}^H$ time is a volume property providing information on the surrounding area of the site to a distance of approximately 2 nm.[61]

Both the ^{1}H−^{13}C and ^{1}H−^{29}Si VCT CP/MAS kinetics curves have been fitted according to eq 2. We note that the ^{1}H−^{13}C CP/MAS kinetics curves give unsatisfactory results when fitted using either eq 2 or a more complex model relying on the presence of a heterogeneous ^{1}H population (I−I*−S model).[37] The unusual CP−dynamics curves observed for the −CH_2CH_2− and −CH=CH− bridges (Figure 9 and Supporting Information) can only be explained using a model where two components with different T_{IS} and $T_{1\rho}^H$ times are identified depending on the mobility of the CP-determining ^{1}H source spins. The "rigid" component displays extremely short T_{CP} and $T_{1\rho}^H$ times, and the "mobile" component shows much longer T_{CP} and $T_{1\rho}^H$ times. The fast CP of the rigid components is a result of directly attached protons with reduced mobility and is indicative of a strong ^{1}H−^{13}C heteronuclear dipolar coupled network, thus representing organic bridges embedded in the bulk of hybrid pore walls. The mobile/slow component can be attributed to organic bridges located at the pore wall interface. In all five products analyzed, the rigid/fast component of the −CH_2CH_2− and −CH=CH− bridges showed similar T_{CP} and $T_{1\rho}^H$ times irrespective of prehydrolysis conditions. This indicates that CP transfer from ^{1}H to ^{13}C is dominated by the directly attached protons and does not rely on the through space heteronuclear coupling to hydroxyl groups or adjacent organic bridges. The $T_{1\rho}^H$ times for the "mobile" component of the −CH_2CH_2− bridges are shorter for S-PMOs compared to those for the J-PMOs (Supporting Information, Table S2). This observation relates to a decrease in mobility of the

(56) Hunger, M. *Solid State Nucl. Magn. Reson.* **1996**, *6*, 1–29.
(57) Abelmann, K.; Totsche, K. U.; Knicker, H.; Kogel-Knabner, I. *Solid State Nucl. Magn. Reson.* **2004**, *25*, 252–266.
(58) Khimyak, Y. Z.; Klinowski, J. *Phys. Chem. Chem. Phys.* **2001**, *3*, 2544–2551.
(59) Khimyak, Y. Z.; Klinowski, J. *Phys. Chem. Chem. Phys.* **2001**, *3*, 616–626.
(60) Jones, M. D.; Duer, M. J.; Hermans, S.; Khimyak, Y. Z.; Johnson, B. F. G.; Thomas, J. M. *Angew. Chem., Int. Ed.* **2002**, *41*, 4726–4729.
(61) McBrierty, V. J.; Douglass, D. C. *Macromol. Rev.* **1981**, *16*, 295–366.

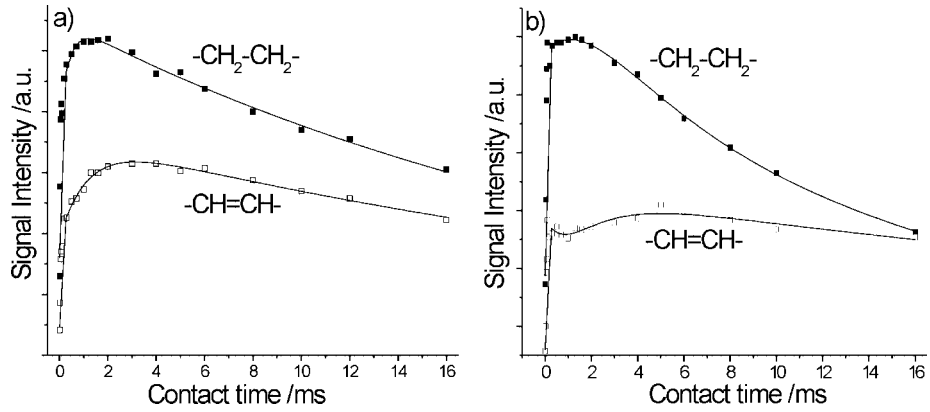

Figure 9. $^{1}H-^{13}C$ CP/MAS kinetics curves of the template extracted PMOs: (a) $-CH_2CH_2-$/$-CH=CH-$PMO and (b) S-PMO-60.

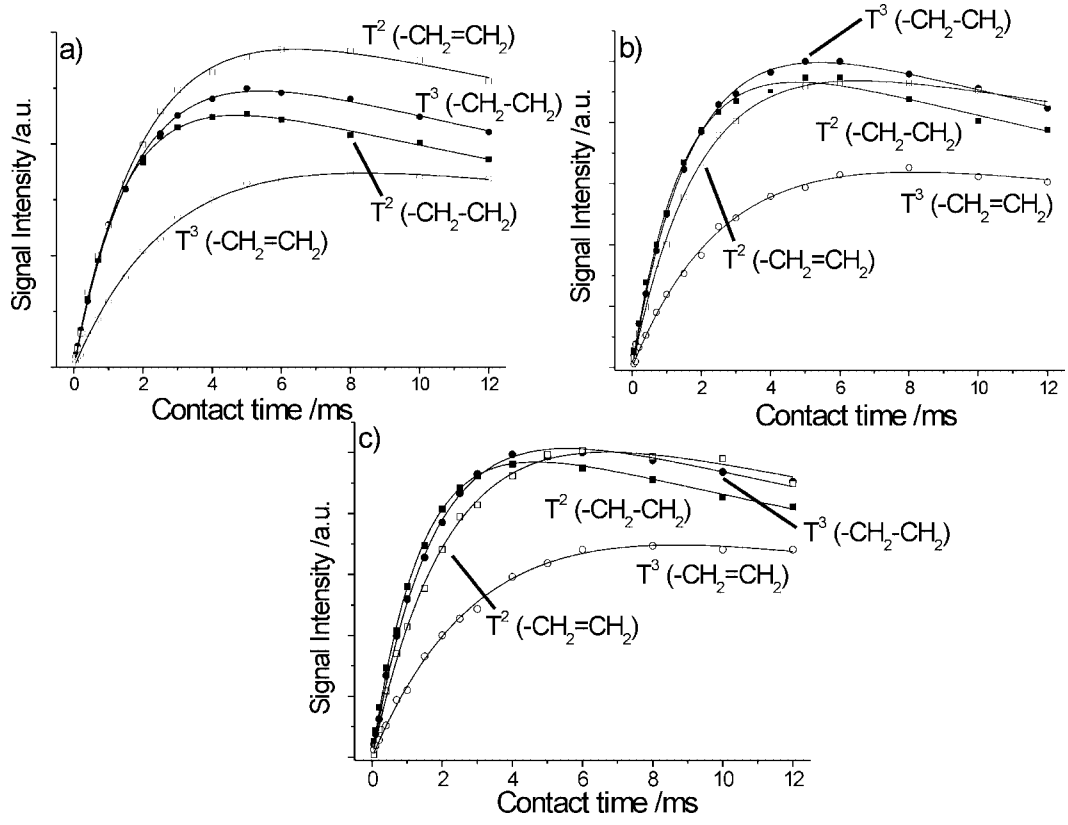

Figure 10. $^{1}H-^{29}Si$ CP/MAS NMR kinetics curves of the template extracted PMOs: (a) $-CH_2CH_2-$/$-CH=CH-$PMO, (b) J-PMO-30, and (c) J-PMO-60.

protons on the organic bridges acting as a CP source. Thus the $-CH_2CH_2-$ bridges at the pore wall interface of S-PMOs are in a more rigid environment. Changes in the mobility of $-CH_2CH_2-$ protons on the pore wall interface, when separate prehydrolysis is used, could originate from the formation of mono-functional organosilica SBUs and, subsequently, domain type structures. However, no significant changes were observed for the $-CH=CH-$ bridges on the pore wall interface irrespective of hydrolysis conditions.

The longer T_{CP} times observed for both the fast and slow components of the $-CH=CH-$ bridges compared to those for the $-CH_2CH_2-$ bridges are a result of fewer protons acting as CP sources. The increase in T_{CP} times of the slow/mobile component compared to the "rigid" component results from a decrease in magnitude of $^{1}H-^{13}C$ heteronuclear dipolar coupling as a function of site mobility.

$^{1}H-^{29}Si$ CP/MAS Kinetics. $^{1}H-^{29}Si$ CP-kinetics curves for the $-CH_2CH_2-$/$-CH=CH-$PMO, J-PMO-30, and J-PMO-60 (Figure 10, Table 3) show much shorter T_{CP} for the $-CH_2-CH_2-$ $T^{2,3}$ silica sites compared to those of the $-CH=CH-$ $T^{2,3}$ sites. This is due to the difference in the number of protons in the organic bridges able to act as CP sources. Shorter T_{CP} times for the T^2 sites compared with those for the T^3 sites can be explained by the presence of directly bound OH group on the T^2 sites facilitating CP build up. The difference in T_{CP} times of $T^{2,3}$ sites bound to their respective organic bridges is more pronounced for the products of separate prehydrolysis protocols (Figure 11, Table 3). For example, in S-PMO-60 the T_{CP} times for T^3 sites connected to $-CH=CH-$ and $-CH_2-CH_2-$ bridges are 3.26 and 1.58 ms respectively. Analogous J-PMO-60 prepared using joint prehydrolysis protocol shows T_{CP} times

Table 3. $^{1}H-^{29}Si$ CP/MAS Kinetics Parameters for the Template Extracted PMOs

resonance, ppm	^{29}Si site	signal intensity[a]	T_{IS}, ms	$T_{1\rho}^{H}$, ms	R^2
		$-CH_2CH_2-/-CH=CH-$PMO			
−56.6	$-CH_2CH_2-$ T^2	1.06 ± 0.01	1.49 ± 0.04	30.1 ± 1.8	0.999
−64.3	$-CH_2CH_2-$ T^3	1.18 ± 0.02	1.80 ± 0.05	30.7 ± 2.4	0.999
−73.4	$-CH=CH-$ T^2	1.34 ± 0.01	2.07 ± 0.04	38.9 ± 2.4	0.998
−81.9	$-CH=CH-$ T^3	0.839 ± 0.01	2.86 ± 0.06	45.1 ± 4.0	0.998
		J-PMO-30			
−57.6	$-CH_2CH_2-$ T^2	1.09 ± 0.03	1.51 ± 0.07	30.3 ± 3.4	0.998
−64.3	$-CH_2CH_2-$ T^3	1.19 ± 0.02	1.78 ± 0.05	31.1 ± 2.1	0.999
−73.2	$-CH=CH-$ T^2	1.07 ± 0.02	1.96 ± 0.07	47.9 ± 6.9	0.999
−81.4	$-CH=CH-$ T^3	0.77 ± 0.01	2.73 ± 0.07	44.7 ± 2.3	0.999
		J-PMO-60			
−56.5	$-CH_2CH_2-$ T^2	1.11 ± 0.02	1.41 ± 0.04	33.9 ± 3.0	0.999
−64.1	$-CH_2CH_2-$ T^3	1.19 ± 0.01	1.76 ± 0.02	35.6 ± 2.1	0.998
−72.9	$-CH=CH-$ T^2	1.19 ± 0.01	2.22 ± 0.05	38.4 ± 1.6	0.998
−81.1	$-CH=CH-$ T^3	0.865 ± 0.009	3.14 ± 0.08	40.1 ± 1.9	0.998
		S-PMO-30			
−57.6	$-CH_2CH_2-$ T^2	1.10 ± 0.02	1.44 ± 0.05	21.7 ± 1.4	0.998
−64.3	$-CH_2CH_2-$ T^3	1.20 ± 0.03	1.76 ± 0.07	22.5 ± 1.9	0.998
−73.2	$-CH=CH-$ T^2	1.35 ± 0.03	2.43 ± 0.08	38.1 ± 4.2	0.999
−81.4	$-CH=CH-$ T^3	1.02 ± 0.01	3.56 ± 0.09	38.3 ± 1.7	0.998
		S-PMO-30			
−57.0	$-CH_2CH_2-$ T^2	1.14 ± 0.03	1.38 ± 0.07	23.7 ± 2.4	0.996
−64.0	$-CH_2CH_2-$ T^3	1.18 ± 0.04	1.58 ± 0.04	27.7 ± 1.8	0.999
−72.9	$-CH=CH-$ T^2	1.27 ± 0.01	2.28 ± 0.04	45.5 ± 1.6	0.999
−81.3	$-CH=CH-$ T^3	0.99 ± 0.01	3.27 ± 0.06	45.1 ± 1.8	0.999

[a] All resonance intensities are normalized to that of $-CH_2CH_2-$ T^3 site at its maximum is equal to 1.

Table 4. Intensities of Cross-Peaks in the $^{1}H-^{29}Si$ HETCOR NMR Spectra[a]

	^{29}Si resonance			
	$-CH_2CH_2-$		$-CH=CH-$	
^{1}H resonance	T^2	T^3	T^2	T^3
	$-CH_2CH_2-/-CH=CH-$PMO			
$-CH_2CH_2-$	0.952	1.00	0.591	0.288
$-CH=CH-$	0.326	0.414	0.573	0.429
(auto peak $T^2 + T^3$)/(cross-peak $T^2 + T^3$)	2.64		1.14	
	J-PMO-30			
$-CH_2CH_2-$	1.11	1.00	0.592	0.298
$-CH=CH-$	0.473	0.512	0.665	0.514
(auto peak $T^2 + T^3$)/(cross-peak $T^2 + T^3$)	2.14		1.32	
	J-PMO-60			
$-CH_2CH_2-$	1.04	1.00	0.460	0.252
$-CH=CH-$	0.367	0.433	0.692	0.521
(auto peak $T^2 + T^3$)/(cross-peak $T^2 + T^3$)	2.55		1.70	
	S-PMO-30			
$-CH_2CH_2-$	1.07	1.00	0.458	0.186
$-CH=CH-$	0.202	0.234	0.680	0.584
(auto peak $T^2 + T^3$)/(cross-peak $T^2 + T^3$)	4.75		1.96	
	S-PMO-60			
$-CH_2CH_2-$	0.984	1.00	0.400	0.107
$-CH=CH-$	0.081	0.124	0.647	0.524
(auto peak $T^2 + T^3$)/(cross-peak $T^2 + T^3$)	9.68		2.31	

[a] Values are normalized to those of the $-CH_2CH_2-$ T^3 resonance.

3.14 ms for $-CH=CH-$ and 1.76 ms for $-CH_2CH_2-$ T^3 sites. The difference in T_{CP} times is less pronounced for the reference solid prepared with no prehydrolysis. This small change indicates a difference in the local environment of the silicon sites when separate prehydrolysis is used in comparison to joint prehydrolysis.

The $T_{1\rho}^{H}$ times are faster for the $-CH_2CH_2-$ $T^{2,3}$ sites compared to the $-CH=CH-$ $T^{2,3}$ sites (Figures 10 and 11). The difference in $T_{1\rho}^{H}$ relaxation times between $-CH_2-CH_2-$ and $-CH=CH-$ T sites is reduced as prehydrolysis time increases in the jointly prehydrolyzed materials (Table 3). This may indicate an increase in homogeneity of distribution of the organic functionalities within the framework. As the time of joint prehydrolysis increases from 30 to 60 min, the hetero co-condensation of organosilica precursors becomes significant. This is reversed for the separately prehydrolyzed PMOs in which the difference in $T_{1\rho}^{H}$ times between the T sites of the two organic groups increases with the prehydrolysis time (Table 3), thus indicating an increased segregation of the organic groups within the mesostructure. Such a domain structure results from the formation of monofunctional

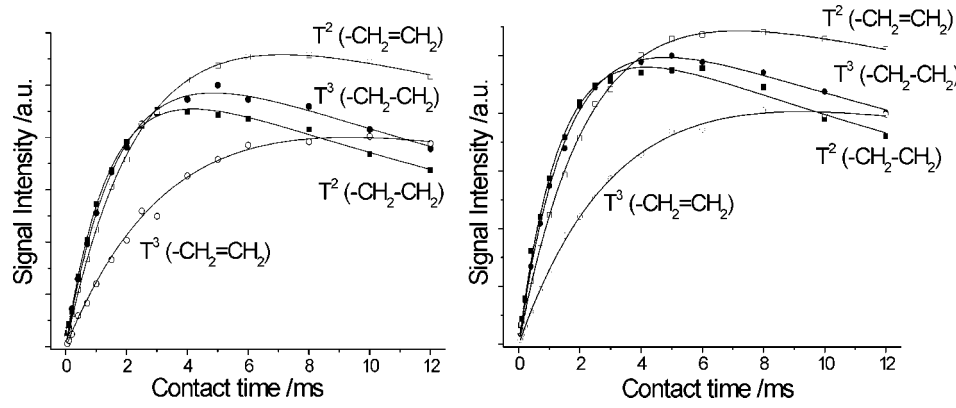

Figure 11. $^{1}H-^{29}Si$ CP/MAS NMR kinetics curves of the template extracted PMOs: (a) S-PMO-30 and (b) S-PMO-60.

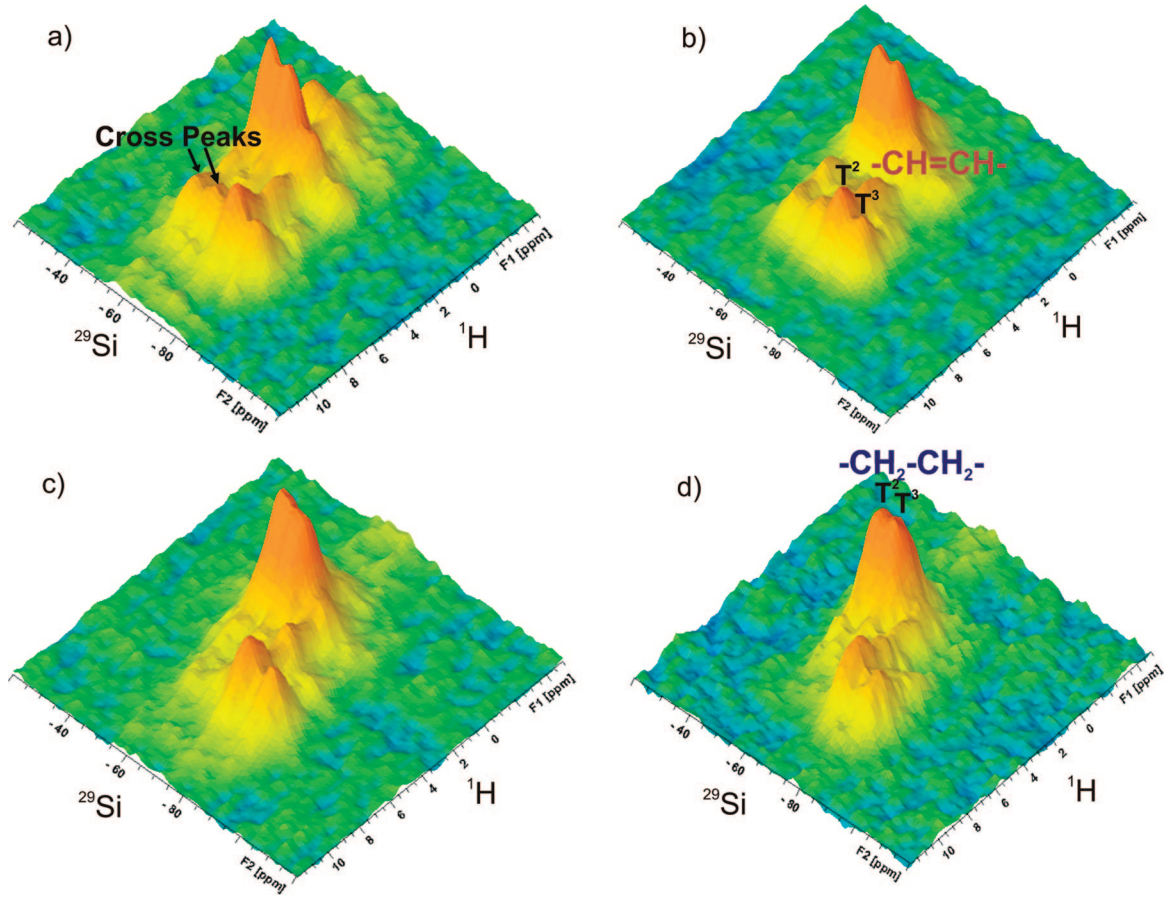

Figure 12. $^{1}H-^{29}Si$ HETCOR NMR spectra of the template extracted PMOs: (a) J-PMO-30, (b) J-PMO-60, (c) S-PMO-30, and (d) S-PMO-60.

organosilica SBUs. Comparing the $T_{1\rho}^{H}$ values of prehydrolyzed PMOs to the reference material (—CH_2CH_2—/—CH=CH—PMO), it is clear that the two materials prepared using separate prehydrolysis are less homogeneous in structure compared to the reference material.

$^{1}H-^{29}Si$ HETCOR NMR. 2D $^{1}H-^{29}Si$ HETCOR experiments provide detailed information on the spatial proximity of the two organic functionalities. The HETCOR spectrum correlates ^{29}Si resonances to ^{1}H sites in their close proximity. The spectra for the —CH_2—CH_2—/—CH=CH—PMO, J-PMO-30, and J-PMO-60 (Figure 12, Supporting Information) show the same silicon $T^{2,3}$ sites as those in the 1D $^{1}H-^{29}Si$ CP/MAS (discussed above) in f_2 correlated to the FSLG decoupled ^{1}H MAS spectrum in the f_1 dimension. The ^{1}H dimension shows four resonances. The resonance at 0.8 ppm is attributed to surface hydroxyl groups, a common observation in ^{1}H MAS NMR spectra of zeolitic materials.[62,63] The ^{1}H resonance at 1.8 ppm from the —CH_2—CH_2— organic bridge correlates to the silicon peaks at −56.6 and −64.3 ppm confirming the assignment of ^{1}H MAS NMR spectra. The peak at 6.8 ppm attributable to the —CH=CH— bridges correlates with the silicon T sites at −73.4 and −81.9 ppm. These autopeaks are expected. In addition, cross-peaks correlating the —CH_2—CH_2— bridge ^{1}H resonance to the —CH=CH— silicon $T^{2/3}$ sites and vice versa are seen. This is indicative of a homogeneous random distribution of organic functionalities in the

framework. Differences in cross-peak intensities are observed in the HETCOR spectra for the jointly prehydrolyzed solids and for the reference $-CH_2-CH_2-$/$-CH=CH-$PMO (Table 4). For the jointly prehydrolyzed PMOs (Figure 12, top) an increase in cross-peak intensity between the silicon $-CH_2CH_2-$ $T^{2,3}$ sites and the proton $-CH=CH-$ site is observed. This suggests that the jointly prehydrolyzed material frameworks are more homogeneous compared to the reference material as indicated by $^1H-^{29}Si$ VCT CP/MAS data (Figure 10, Table 3). The cross-peak for the ^1H resonance at approximately 4.2 ppm to all four silicon sites confirms its assignment as H-bonded water molecules close enough in space to the silicon sites to act as CP "donors". An H_2O peak is observed at approximately 4.2 ppm in the ^1H MAS NMR spectra although its intensity is reduced in the HETCOR experiments.

The $^1H-^{29}Si$ HETCOR spectra of the S-PMO-30 and S-PMO-60 show a decreased intensity of the peak of the surface hydroxyl group at 0.8 ppm upon increased prehydrolysis time. A reduction in cross-peak intensities for the silicon $-CH_2-CH_2-$ $T^{2,3}$ and $-CH=CH-$ proton resonances along with a similar reduction for correlations between the silicon $-CH=CH-$ and $-CH_2-CH_2-$ proton sites is observed for S-PMOs in comparison to J-PMOs and the reference material (Table 4). This can only be observed if the two different organic bridges are within the same mesoporous framework proving phase purity of S-PMOs. It is clear that a structure with domains consisting preferentially of $-CH_2-CH_2-$ and $-CH=CH-$ functional groups in the same mesoporous framework is formed proving the efficiency of prehydrolysis procedure relying on the co-condensation of mono-organo-functionalized SBUs (Scheme 1).

The HETCOR and $^1H-^{29}Si$ VCT CP/MAS NMR results are complementary and suggest that when joint prehydrolysis is used, the products are similar to the reference material and feature an increasingly homogeneous framework as hydrolysis time increases. For separately prehydrolyzed solids the organic functionalities become increasingly segregated as prehydrolysis time increases. The homogeneity of the products depends on the prehydrolysis conditions, with respect to the predominant co-condensation (homo- vs hetero-condensation of the organosilica precursors), in the formation of organosilane SBUs.

Conclusions

Mesoporous bifunctional $-CH_2-CH_2-$/$-CH=CH-$ PMOs with both organic functionalities incorporated in the same mesoporous framework have been prepared in the presence of a nonionic block copolymer surfactant, using a modified synthetic procedure to control the properties of the products. The distribution of organic groups in PMOs can be controlled using prehydrolysis of organosilica precursors. In joint prehydrolysis conditions a homogeneous distribution of the two organic groups was observed. However, when separate prehydrolysis conditions were used a domain type structure containing segregated regions of $-CH_2CH_2-$ and $-CH=CH-$ bridges within the same mesostructural framework was obtained. The distribution of organic functional groups was confirmed by $^1H-^{29}Si$ HETCOR and VCT CP/MAS NMR. PMOs prepared using both joint and separate prehydrolysis showed high surface areas and large pore volumes with narrow pore size distributions. These properties would make these materials ideal for the use in molecular recognition/separation of medium or large organic molecules. The ability to control the distribution of organic functionalities and characterize the resulting complex porous structure with limited long-range ordering can be considered as a step forward in the synthesis of complex hierarchical materials.

Acknowledgment. The financial support of this work by the EPSRC (Grant EP/C514580/1) is gratefully acknowledged.

Supporting Information Available: PXRD patterns of the as-synthesized and extracted PMOs along with $^{13}C/^{29}Si$ CP MAS, ^{13}C CP/VCT MAS, and ^{29}Si MAS (including tables of VCT and Gaussian deconvolution parameters), $^1H-^{29}Si$ HETCOR of template extracted $-CH_2CH_2-$/$-CHCH-$PMO, and nitrogen adsorption−desorption isotherms (PDF). This material is available free of charge via the Internet at http://pubs.acs.org.

CM7036124

(62) Klinowski, J. *Chem. Rev.* **1991**, *91*, 1459–1479.
(63) Klinowski, J. *Annu. Rev. Mater. Sci.* **1988**, *18*, 189–218.